Hoar crystal development and disappearance at Dome C, Antarctica: observation by near-infrared photography and passive microwave satellite

Nicolas Champollion, Ghislain Picard, Laurent Arnaud, E. Lefebvre, Michel Fily

The Cryosphere, 7, 1247–1262, 2013
www.the-cryosphere.net/7/1247/2013/
doi:10.5194/tc-7-1247-2013

The Cryosphere Open Access

Hoar crystal development and disappearance at Dome C, Antarctica: observation by near-infrared photography and passive microwave satellite

N. Champollion, G. Picard, L. Arnaud, E. Lefebvre, and M. Fily

UJF – Grenoble 1 / CNRS, Laboratoire de Glaciologie et Géophysique de l'Environnement (LGGE) UMR5183, Grenoble, 38041, France

Correspondence to: N. Champollion (nicolas.champollion@lgge.obs.ujf-grenoble.fr)

Received: 29 October 2012 – Published in The Cryosphere Discuss.: 10 January 2013
Revised: 20 June 2013 – Accepted: 24 June 2013 – Published: 8 August 2013

Abstract. Hoar crystals episodically cover the snow surface in Antarctica and affect the roughness and reflective properties of the air–snow interface. However, little is known about their evolution and the processes responsible for their development and disappearance despite a probable influence on the surface mass balance and energy budget. To investigate hoar evolution, we use continuous observations of the surface by in situ near-infrared photography and by passive microwave remote sensing at Dome C in Antarctica. From the photography data, we retrieved a daily indicator of the presence/absence of hoar crystals using a texture analysis algorithm. The analysis of this 2 yr long time series shows that Dome C surface is covered almost half of the time by hoar. The development of hoar crystals takes a few days and seems to occur whatever the meteorological conditions. In contrast, the disappearance of hoar is rapid (a few hours) and coincident with either strong winds or with moderate winds associated with a change in wind direction from southwest (the prevailing direction) to southeast. From the microwave satellite data, we computed the polarisation ratio (i.e. horizontal over vertical polarised brightness temperatures), an indicator known to be sensitive to hoar in Greenland. Photography data and microwave polarisation ratio are correlated, i.e. high values of polarisation ratio which theoretically correspond to low snow density values near the surface are associated with the presence of hoar crystals in the photography data. Satellite data over nearly ten years (2002–2011) confirm that a strong decrease of the polarisation ratio (i.e. signature of hoar disappearance) is associated with an increase of wind speed or a change in wind direction from the prevailing direction. The photography data provides, in addition, evidence of interactions between hoar and snowfall. Further adding the combined influence of wind speed and wind direction results in a complex picture of the snow–atmosphere interactions in Antarctica which deserves further quantification and modelling.

1 Introduction

Many observers have noticed the frequent presence of hoar crystals at the surface in Greenland (Shuman et al., 1993) and in Antarctica (Gow, 1965; Orheim, 1968; Linkletter and Warburton, 1976; Gallet et al., 2011). Since these crystals are very different from the snow grains usually present at the surface, they can dramatically change the properties of the air–snow interface, that is, the density and optical grain radius of the first centimetres of snow below the surface, and the surface roughness (Shuman et al., 1993; Gallet et al., 2011). In particular, the presence of hoar can impact snow albedo that is largely determined by the optical radius of snow particles present at the surface (Flanner and Zender, 2006; Gardner and Sharp, 2010; Gallet et al., 2011; Picard et al., 2012). These crystals also form ideal traps for falling or drifting snow grains (Domine et al., 2012), and therefore have an influence on snow settling (Zwaaftink et al., 2012) which is important to determine the surface mass balance (Arthern et al., 2006; Eisen et al., 2008; Favier et al., 2011). These

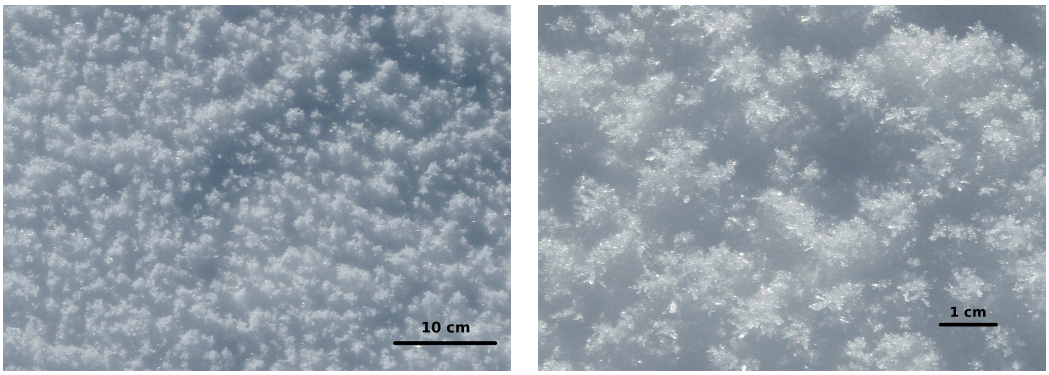

(a) (b)

Fig. 1. Pictures of hoar at Dome C: **(a)** wide view **(b)** close view. Taken by hand with a normal camera on 30 December 2011.

crystals may also influence the snow chemistry, by influencing the ice surface over volume ratio and density (Domine and Shepson, 2002). However, the precise nature of these crystals (Fig. 1) – either surface hoar (Fierz et al., 2009) or frost flowers (Style and Worster, 2009) – and the processes leading to their development and disappearance are uncertain. The atmospheric and weather conditions are intuitively an important driver (Gow, 1965; Orheim, 1968; Linkletter and Warburton, 1976; Bromwich, 1988; Shuman et al., 1993) but the determination of the respective roles of temperature, humidity and wind have received little attention so far.

The objective of this study is to characterise the evolution of the hoar cover at the surface at Dome C (75°06′ S, 123°21′ E; Fig. 2) in the East Antarctic Plateau and to relate this evolution to weather conditions. To this end, we use two sets of continuous observations of the air–snow interface, as well as weather observations.

The first set of observations comes from a near-infrared camera installed at Dome C to provide hourly pictures of the surface. Operating in the near-infrared domain where the sensitivity to snow grain size is maximal (Domine et al., 2006) provides sharp pictures where hoar crystals and other features can be visually identified. We developed an automatic algorithm to detect changes of picture texture and hence produced a 2 yr long, objective and accurate time series of hoar presence. To extend this series in time and space, we exploited a second set of observations derived from brightness temperatures (T_B) measured by passive microwave remote sensing. Brightness temperatures are mainly sensitive to the snowpack while the atmosphere is negligible at the frequencies of 19 and 37 GHz used here (Picard et al., 2009; Brucker et al., 2011). Despite the penetration depth which is of the order of metres at these frequencies (Surdyk, 2002a; Macelloni et al., 2007), using a combination of T_B at different polarisations can emphasise the sensitivity to the properties of the air–snow interface. Shuman et al. (1993) computed two indexes, the T_B ratio of vertical over horizontal polarisations, and the T_B difference of both polarisations. They found that both were related to the near-surface density, the surface grain-scale roughness (roughness with wavelength and amplitude in the order of the snow grain size, around 1 cm, in Shuman et al., 1993) and the presence of hoar. Surdyk (2002b), by using a similar indicator (i.e. the normalised difference between T_B at vertical and horizontal polarisation) showed that it was influenced by both the internal stratification of the snowpack and the air–snow interface. However, since the temporal variations of the former factor are slow in Antarctica (Arthern et al., 2006), the indicator is useful to monitor the variations of the air–snow interface properties. Therefore, polarimetric combinations of passive microwave data are sensitive to density variations of the snow near the surface and hence to the presence of hoar.

Section 2 presents the datasets used in this study, and explains the method applied to detect hoar crystals from photography and microwave data. Section 3 presents the results on the presence of hoar crystals and analyses the conditions of their development and disappearance.

2 Materials and methods

The following sections describe the two datasets used to detect hoar presence and the auxiliary dataset used to determine the role of weather conditions in hoar evolution.

2.1 In situ near-infrared photographs

2.1.1 Experimental device

Near-infrared pictures are taken at Dome C every hour using an experimental device called PAuto. The device is composed of a camera (Canon EOS 5D) pointing downward perpendicularly to the horizontal surface, an embedded computer to adjust camera settings and perform picture acquisition and transmission, and a global positioning system for accurate time synchronisation. PAuto is packaged in a heated box to support the −70 to −80 °C of the Dome C winter. It is

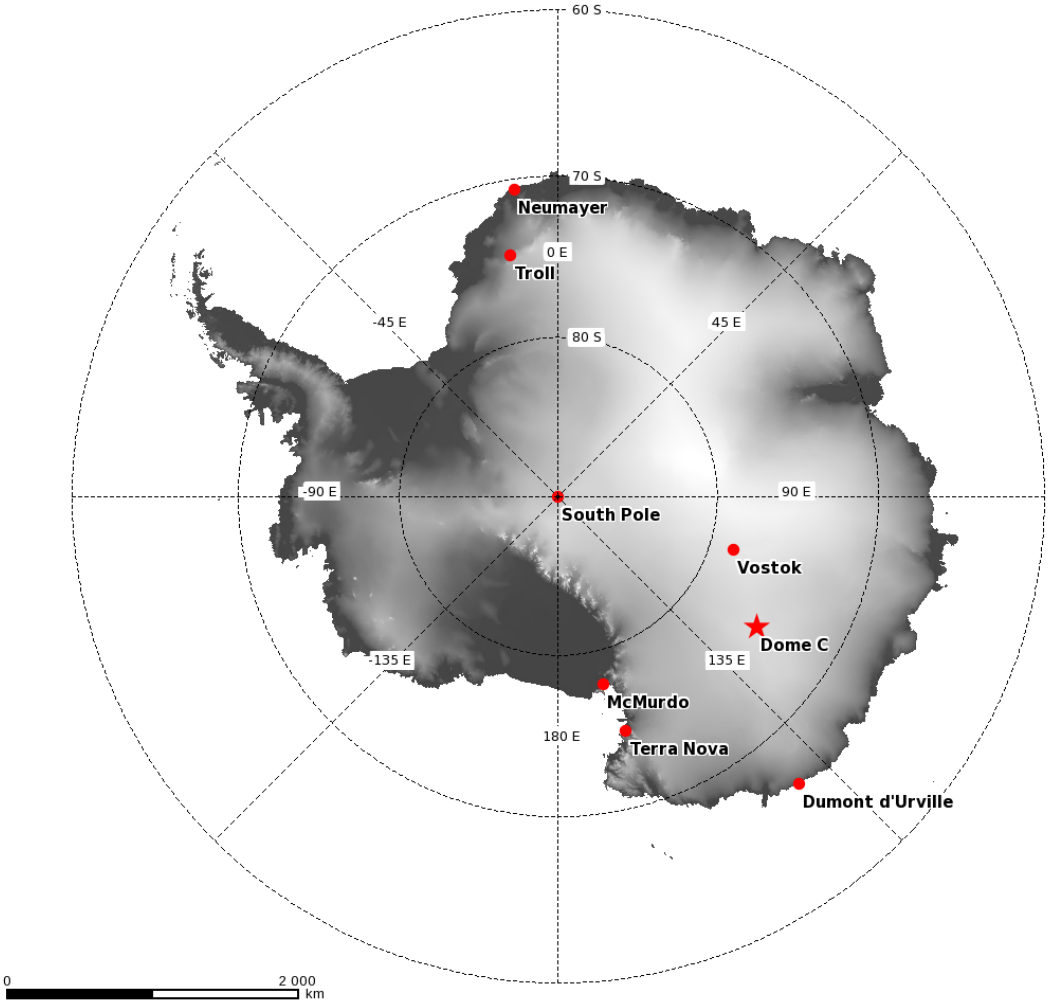

Fig. 2. Location of Dome C on a geographic map of Antarctica.

suspended 2 m above the snow surface (Fig. 3) and equipped with a 50 mm fixed focal lens which gives an imaged area of about 4 m^2. The camera sensor is filtered in the near-infrared range on a wavelength greater than 835 nm. PAuto was set up about 1 km away from the Concordia base on 23 November 2009 in an undisturbed area, and operated until 16 February 2010 when the camera stopped working. A second camera was set up on 3 January 2011 and is still running (as of 11 April 2012). The picture acquisition during the polar night is possible with artificial infrared lighting (850 nm wavelength) hitched up to the posts on either side of the camera.

Hoar crystals on the snow surface are clearly identifiable from the pictures (Fig. 4a, b, d). Our objective is to derive a Boolean indicator of the presence/absence of hoar, even though in the future the percentage of hoar cover at the surface may be accessible. Figure 4a and d illustrate cases where small-scale heterogeneities and grainy, highly textured pictures are observed. This case corresponds to the presence of hoar crystals. In contrast, Fig. 4b shows a smooth and regular surface with only large-scale structures but no hoar. Our algorithm of automatic detection is based on the small-scale texture.

2.1.2 Hoar crystal detection from picture texture analysis

From the grey level co-occurrence matrix GLC matrix defined in Haralick et al. (1973); He et al. (1988); Hall-Beyer (2007), many approaches of texture analysis are possible such as contrast index, homogeneity index, energy and entropy. In our case, the approaches based only on the individual pixel values (grey level histogram or image filtering, Serra, 1984, 1988) are insufficient. Therefore, we combined the texture-based approach (GLC matrix calculation) and image filtering. The algorithm is composed of five steps.

1. Conversion of the original image to greyscale using a normalised linear combination of the red, green

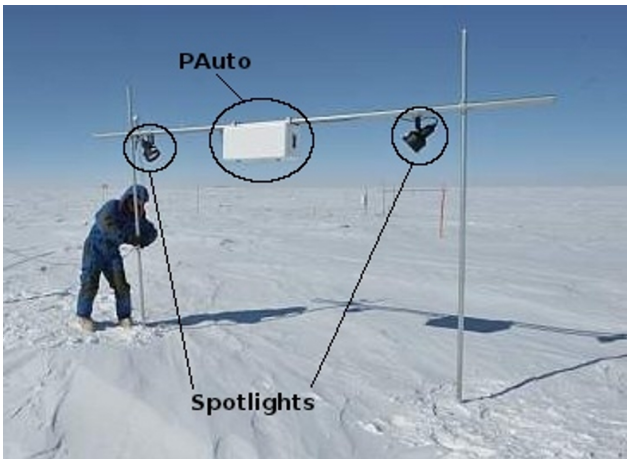

Fig. 3. PAuto: experimental device taking hourly near-infrared pictures of the snow surface at Dome C. The white box contains the camera, computer, GPS and heating. The two near-infrared spotlights provide illumination during the night.

and blue bands based on the human perception of colours (Plataniotis and Venetsanopoulos, 2000). Filtering of the three colour bands of the camera sensor (greater than 835 nm) gives more sensitivity to the near-infrared, and, in addition, combining the three rather than selecting a single band, reduces noise by averaging.

2. Elimination of the picture if taken under cloudy conditions. As shown in Fig. 4c, the contrast in pictures – estimated using the standard deviation – on a cloudy day is 2–5 times less than on a clear sky day, and the surface state cannot be accurately determined. A cloudy day is detected based on a threshold on the standard deviation which was determined empirically. The pictures by night taken under artificial illumination are not affected by clouds.

3. High-pass spatial filtering of the greyscale image I to eliminate the large-scale structures. Using a Gaussian kernel, the filtered image I^* is computed as follows:

$$I^*(x,y) = (I \star (1-\phi))(x,y) = \sum_{k=1}^{n}\sum_{l=1}^{m} I(x-k, y-l)(1-\phi(k,l)), \quad (1)$$

$$\phi(x,y) = \frac{1}{2\pi\sigma^2}\exp\left(\frac{-x^2+y^2}{2\sigma^2}\right), \quad (2)$$

where $\star$ is the convolution product operator. σ is the standard deviation of the Gaussian kernel ϕ, x and y are the image coordinates, and n and m are the image dimensions.

4. Calculation of the contrast index C as follows: first, the normalised GLC matrix G and GLC symmetric matrix G_{sym} of the filtered image are obtained by

$$G_{\Delta x,\Delta y}(i,j) = \sum_{x=1}^{n}\sum_{y=1}^{m} \begin{cases} 1, \text{ if } I^*(x,y) = i \text{ and} \\ \quad I^*(x+\Delta x, y+\Delta y) = j \\ 0, \text{ otherwise,} \end{cases} \quad (3)$$

$$G_{\mathrm{sym}\ \Delta x,\Delta y} = G_{\Delta x,\Delta y} + G_{-\Delta x,-\Delta y}, \quad (4)$$

where the pair $(\Delta x, \Delta y)$ is the offset, and i and j are pixel values (from 1 to 256).
Second, the sum of G_{sym} (noted G^*_{sym}) is calculated for offsets between 0 and a maximum value S, which depends on the size of the pattern and orientation to detect, and is discussed hereinafter. In our case, the hoar crystals on the pictures have no prevailing orientation and their maximum extent is between 5 and 10 pixels. G^*_{sym} is given by

$$G^*_{\mathrm{sym}} = \sum_{\Delta x=1}^{S}\sum_{\Delta y=0,1} G_{\mathrm{sym}\ \Delta x,\Delta y}. \quad (5)$$

Third, the symmetric and normalised GLC matrix P is calculated by

$$P(i,j) = \frac{G^*_{\mathrm{sym}}(i,j)}{\sum_{i,j=1}^{N} G^*_{\mathrm{sym}}(i,j)}, \quad (6)$$

where N is the maximum pixel value (256), and the size of P is $N \times N$. Lastly, the contrast index C is

$$C = \sum_{i,j=1}^{N} P(i,j)\,(i-j)^2\,. \quad (7)$$

5. Determination of the surface state depending on C. Because of changes in surface illumination throughout the year, the algorithm is slightly different depending on whether the illumination is natural or artificial. To produce a daily time series, one picture is selected every day among the 24 available. When the sun is above the horizon, the illumination varies significantly during the day. The picture of the day is then selected so that the sun zenith angle is as constant as possible. In practice, we chose the range 80–85°, which gives the same appearance as on the 2 January 2010 picture (Fig. 4a), to cover the longest period possible. This period, where the illumination is natural, called "summer" hereinafter, extends from 1 September to 11 April at Dome C (−75° S). The rest of the year (called "winter"), the illumination is artificial and almost constant.

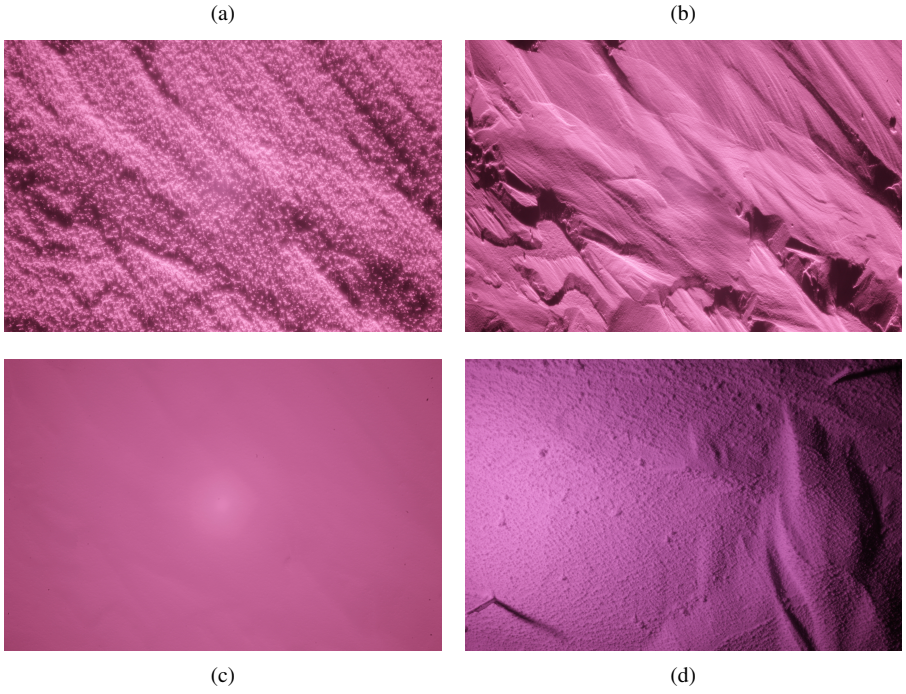

Fig. 4. Near-infrared pictures at Dome C: **(a)** surface with hoar on 2 January 2010; **(b)** smooth surface on 25 November 2009; **(c)** picture under cloudy conditions on 16 December 2009; **(d)** surface with hoar on 15 June 2011.

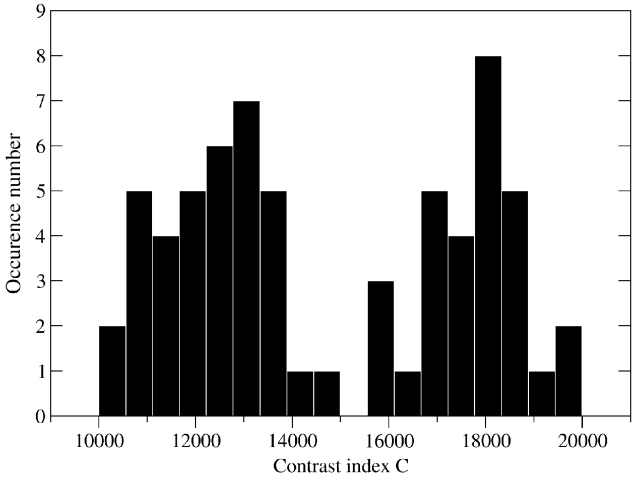

Fig. 5. Histogram of the contrast index (C), which depends on the texture of surface pictures, for the 2009–2010 summer period.

We selected the picture that maximises the standard deviation on greyscale images, such as the 15 June 2011 picture (Fig. 4d). The histograms of C values for both periods are clearly bimodal (as example, see the histogram for the 2009–2010 summer period in Fig. 5) but under natural illumination the hoar-covered pictures correspond to the lower mode while the opposite is observed in artificial illumination. Hence, the algorithm determines the presence of hoar based on whether the C value is lower for the summer period (conversely higher for the winter period) than a given threshold. The threshold value is chosen at the minimum between the two modes and is determined independently for each period. We compared the two flavours of the algorithm during periods where natural and artificial illuminations coexist and found exactly the same results. The difference between the mode which corresponds to hoar-covered pictures under natural and artificial illumination (respectively summer and winter periods) comes from the inhomogeneity of the illumination throughout the picture when it's artificial (Serra, 1984, 1988; Di Siquiera et al., 2013).

The time series of surface state is calculated by running the algorithm separately for each period (three "summers" and one "winter"). The parameters, σ for the Gaussian kernel and S for the GLC matrix offset, are found by maximising the difference between the contrast indexes of pictures selected empirically based on clearly contrasted surface states. The values $\sigma = 5$, 6 and 7; $S = 5$ were found for the three summer periods, respectively, and $\sigma = 1$; $S = 25$ for the winter period. The particular selection has almost no influence on these values.

The resulting 415 day long time series is finally compared with the surface state determined by visual inspection of the near-infrared pictures. Automatic and manual determinations agree in 85 % of cases. The discrepancy has several possible causes: (1) few pictures on cloudy days pass step 2 of the

algorithm; (2) if hoar crystals at the surface are too small or sparse, the algorithm tends to classify the picture as smooth (no hoar); (3) sometimes snow falling from the PAuto box tends to cause a classification as smooth. In the following, we use a corrected time series when the cause is (1) or (3). Case (2) correspond to an ambiguity. For example, hoar crystals on the snow surface are obviously small and sparse at the beginning of their development. Therefore, the day where the surface is manually classified with hoar could easily change by 2 days depending on the operator. The corrected time series of surface state is finally consistent with manual detection in 94 % of cases.

2.2 Passive microwave satellite observations

Passive microwave observations were acquired at 18.7 and 36.5 GHz by the Advanced Microwave Scanning Radiometer – Earth observing system (AMSR-E) in dual-polarisation mode, vertically and horizontally, from 19 June 2002 to 3 October 2011 when the radiometer stopped operating. Daily-averaged brightness temperatures in the pixel including the Concordia station were extracted from the *AMSR-E/Aqua daily L3 25 km brightness temperature, sea ice concentration, and snow depth polar grids dataset* provided by the National Snow and Ice Data Center of the United States. The pixel size is 25 km × 25 km but the effective spatial resolution is slightly different. According to the AMSR-E webpage http://nsidc.org/data/docs/daac/, the total sensor bias error is around 0.6 K. The dataset contains, for every day, the mean of the daily-averaged ascending orbits and daily-averaged descending orbits. At Dome C, owing to the near-polar orbit of the Aqua satellite, there are typically seven over passes per day.

A detailed analysis of the spatial and temporal variability of passive microwave data close to Dome C was given by Long and Drinkwater (2000); Macelloni et al. (2007); Brucker et al. (2011). These studies included the effects of viewing azimuth angle and acquisition time on the satellite observations. Their conclusions are (1) the differences between T_B of the pixel containing the area of in situ measurements (close to the Concordia base) and T_B of the pixels around are weak; (2) the temporal evolutions of T_B of the pixel containing the area of in situ measurements and T_B of the pixels around are similar; (3) the T_B variations induced by the variations of viewing azimuth angle and time, are independent of the season and frequency. Therefore, our study is based on the assumption that the satellite pixel containing in situ measurements is representative of the satellite pixels around Dome C.

To emphasise the sensitivity to snow surface, we derived the polarisation ratios (PR) at 19 and 37 GHz by

$$PR_\nu = \frac{T_B(\nu, h)}{T_B(\nu, v)}, \quad (8)$$

where $T_B(\nu, \alpha)$ is the brightness temperature, ν the frequency and α the polarisation. Based on the results of Shuman et al. (1993) and the measured thickness of hoar on the surface (1–2 cm), other channels of the AMSR-E satellite, i.e. 6, 10 and 89 GHz, were not used in this study. Wavelengths of the 6 and 10 GHz channels are indeed much larger than the thickness of the surface layer of hoar and conversely for the 89 GHz channel.

To understand PR, it is useful to express T_B as the product between the snowpack effective temperature and the microwave emissivity (Zwally, 1977; Sherjal and Fily, 1994; Picard et al., 2009). Since the former is almost independent of the frequency, PR is approximatively equal to the ratio of horizontal over vertical polarisation microwave emissivity. The emissivity can be further decomposed into a volume component caused by snow scattering and a surface component depending only on the reflection coefficient at the air–snow interface (Surdyk and Fily, 1993). At Dome C, it is reasonable to assume that the volume emissivity is constant at the timescale of a year (Surdyk, 2002a; Brucker et al., 2011). Hence, PR temporal variations are mainly caused by changes of surface reflection coefficients.

In the case of a flat snow–air interface, the reflection is specular, and the reflection coefficients can be calculated with the Fresnel equations (Born and Wolf, 1999) as a function of the incident angle and the real part of the dielectric constant of snow, which mainly depends on the snow density. By construction, the AMSR-E observation zenith angle (54.8°) is close to Brewster's angle for the air–snow interface, which means that the reflection coefficient at vertical polarisation (r_v) approaches zero. Consequently, the polarisation ratio mainly depends on the reflection coefficient at horizontal polarisation (r_h), and as a consequence on the dielectric contrast between snow and air, which mostly depends on snow density near the surface. In principle, surface roughness can also influence the reflection coefficient. The coefficient at vertical polarisation usually increases with increasing roughness, and thus T_B vertically polarised decreases (Liang et al., 2008, 2009). At horizontal polarisation, the effect is more variable but, even if the coefficient increases, it increases less than at vertical polarisation (Tsang et al., 2000; Liang et al., 2009). The polarisation ratio therefore increases with increasing surface roughness. However, Mätzler (2005) explains that the effect of surface roughness on T_B is weak for an observation angle of 55° (which applies to AMSR-E). Furthermore, by comparing passive and active microwave observations, Lacroix et al. (2009) showed that the dependence of the passive microwave signal on snow density is one order of magnitude higher than on surface roughness. Hence, the polarisation ratio is mainly dependent on the snow density near the surface, even if the snow surface is rough.

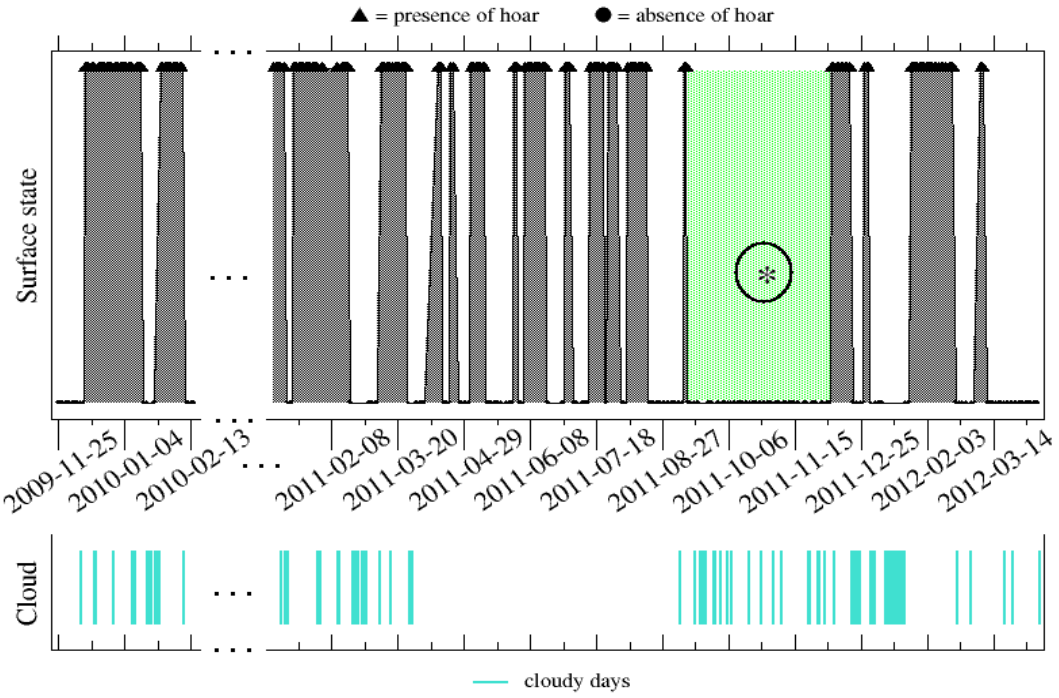

Fig. 6. Evolution of the surface state at Dome C (dark and dotted areas show periods with presence of hoar), from 23 November 2009 to 16 February 2010, and from 3 January 2011 to 11 April 2012. Green and dotted area (*) is a remarkably long period without hoar crystals and cyan lines show cloudy days.

2.3 Weather observations

Weather data used to investigate the conditions of hoar crystal development and disappearance are provided by the automatic weather station program of the Antarctic Meteorological Research Center (Dome C data ARGOS code is 8989 on ftp://amrc.ssec.wisc.edu/pub/aws/10min/rdr/) for the entire period of AMSR-E and photography data. Raw measurements taken every 10 min are used to calculate the daily averages of air temperature (K), wind speed (m s^{-1}), wind direction (°), air pressure (HPa) and humidity (%) after bad values are masked out. Based on the technical manual (Weidner, 1985), wind direction has a resolution of 1.5° and wind speed a resolution of 0.25 m s^{-1} (wind speeds below 0.25 m s^{-1} are considered to be zero). The accuracy of wind direction and speed is twice the resolution.

3 Results and discussion

The following sections analyses the evolution of hoar and its relationship with weather conditions: the first section presents the general characteristics of the time series derived from the near-infrared pictures, and focuses then on the transitions (hoar crystal development and disappearance) and their causes; the second section exploits passive microwave observations to extend these results; and the last section shows evidence of interactions between hoar crystals, albedo and snowfall.

3.1 Observation of hoar crystals from in situ near-infrared photographs

3.1.1 General characteristics

Figure 6 represents the time series of surface state obtained from the near-infrared pictures. The algorithm excluded 77 days with clouds during the summer periods (step 2 of the algorithm), which represents 21 % of the time during the summer periods. This result is in agreement with the annual cloud cover of 22.1 % (Saunders et al., 2009).

The time series shows that the surface state often changes (Fig. 6). The algorithm detects hoar 45 % of the time (187 days) divided into 19 continuous periods during the 18 months of the time series which demonstrates that hoar is far from a marginal phenomenon at Dome C. These periods last between 2 and 35 days. The hoar periods are usually longer in summer than in winter. The periods without hoar generally last between 2 and 25 days. One remarkably long period of 87 days was recorded during the autumn 2011 (see period (*) in Fig. 6).

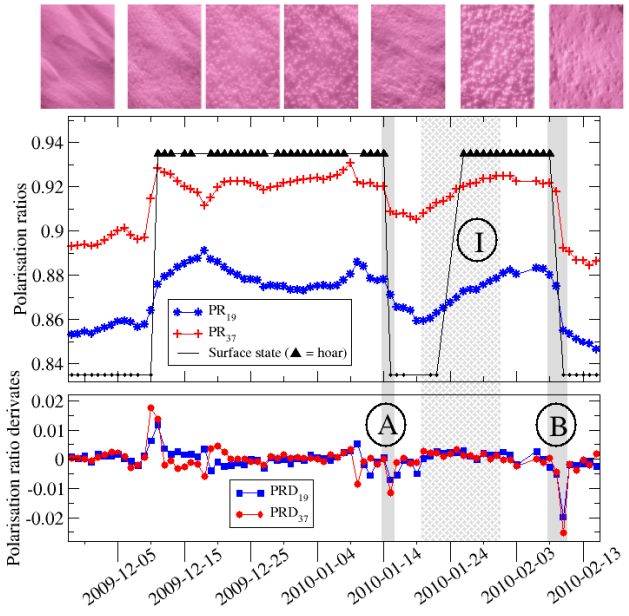

Fig. 7. Evolution of the surface state at Dome C (unscaled black symbols and small pictures above the graph), and time series of polarisation ratios at 19 and 37 GHz and their derivatives (respectively PRD_{19} and PRD_{37}), in December 2009 and January 2010. **(A)** and **(B)** mark two events of hoar crystal disappearance, and **(I)** a period of hoar crystal development.

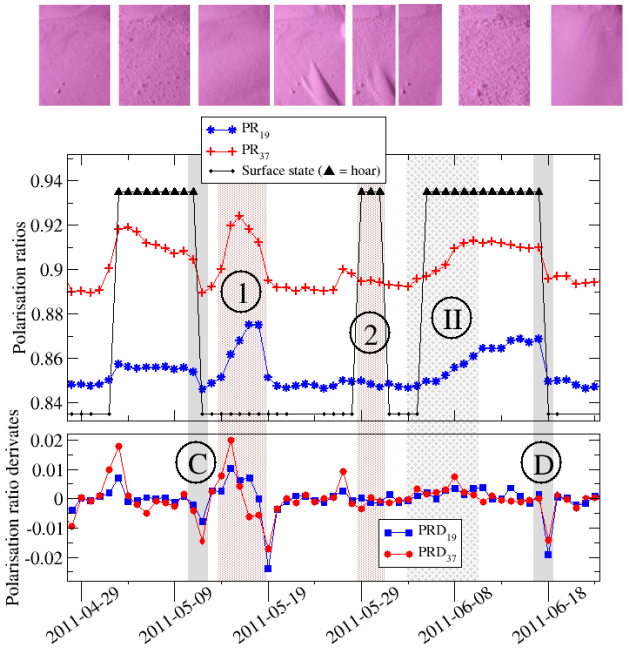

Fig. 8. Evolution of the surface state at Dome C (unscaled black symbols and small pictures above the graph), and time series of polarisation ratios at 19 and 37 GHz and their derivatives (respectively PRD_{19} and PRD_{37}), in May and June 2011. **(C)** and **(D)** mark two events of hoar crystal disappearance, **(II)** is a period of hoar crystal development, and **(1)** and **(2)** are two short periods without correlation between surface state and polarisation ratios.

The following two sections focus on the few days of transition between surface states, i.e. the development and disappearance of hoar.

3.1.2 Hoar crystal development

The development of hoar crystals is observed throughout the 18 months of observation even during the polar winter while the air and snow temperature is low and air contains very little water vapour (Town et al., 2008). Visual inspection of the pictures confirms that the detection algorithm is correct. It also shows that the apparent size of the crystals, and the percent of hoar cover are mostly (not always) lower in winter than in summer.

The development is progressive, for example from 20 to 31 January 2010 and from 3 to 10 June 2011 (see respectively periods I and II in Figs. 7 and 8). In general, it takes around 3 to 6 days to completely cover the surface, usually faster in summer than in winter. There is nothing particular about the weather conditions during this development, or at least we did not identify any significant departure in temperature, pressure or humidity data from periods without development.

The nature of the crystals and the physical processes governing their formation are difficult to determine from the automatic photographs. Nevertheless, in summer, it is evident by visual observations in the field that these crystals are not surface hoar (Fierz et al., 2009), i.e. they are not formed by condensation of the atmospheric humidity onto the surface. In fact, the crystals are composed of many needles and dendritic outgrowths with an irregular structure. A more probable formation process is the condensation of an upward flux of water vapour coming from the underlying snow layers. As suggested by Orheim (1968); Weller (1969); Gallet et al. (2011); Picard et al. (2012), the temperature profile inside the snowpack during summer implies a water vapour flux from the few centimetres under the snow surface towards the atmosphere. It results in "sublimation" crystals growing on the surface like frost flowers (Domine et al., 2005). In winter, this upward flux, essentially driven by the penetration of solar radiation into the snow, is absent. Since hoar development is still observed and even frequent, it is probable that the crystals are of a different nature than in summer. They could be surface hoar formed by water vapour deposition from the atmosphere onto the surface because it is frequent during the polar night that the snow surface is much colder than the air, owing to intense radiative cooling and absence of solar energy. The observation of crystal morphology in the field, which shows hollow facets with shared angles, and the large size of these crystals, support this assumption for the formation process (Slaughter et al., 2011). However, the near-infrared pictures cannot resolve the details of shape, and we cannot confirm these hypotheses except from the fact that

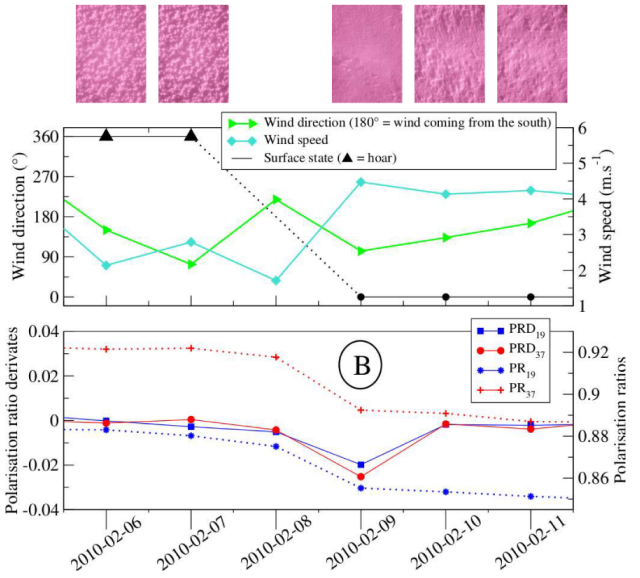

Fig. 9. Disappearance of hoar crystals (unscaled black symbols and small pictures above the graph) present at the surface on 9 February 2010 at Dome C (event B in Fig. 7). Between the 8 and 9, a decrease of polarisation ratios at 19 and 37 GHz and highly negative values of their derivatives (respectively PRD_{19} and PRD_{37}) are observed, as well as a change in wind direction (wind coming from southwest to wind coming from southeast) and a twofold increase of wind speed.

hoar grows all through the year while temperature, energy budget and humidity change dramatically.

3.1.3 Hoar crystal disappearance

In contrast to hoar development, the disappearance of the crystals is usually rapid – less than one day – and occurs during particular events, such as the events (A) on 14 January 2010 and (B) on 9 February 2010 (see Fig. 7), (C) on 11 May 2011 and (D) on 17 June 2011 (see Fig. 8).

Based on the pictures, we never observed a slow evolution or partial disappearance of hoar crystals. Therefore, we estimate that disappearance by sublimation or metamorphism did not happen over the 18 months, probably because of the too low temperature resulting in weak vapour flux (Colbeck, 1983; Taillandier et al., 2007; Town et al., 2008). Even during the period from 20 to 30 January 2010, clearly identified with a negative latent flux (Brun et al., 2011), hoar was present at the surface. The stability of the hoar presence comes from the stability of individual or aggregate crystals. By following the individual evolution of a few crystals, we noticed that they usually develop until they touch their neighbours, and then become remarkably stable until an event occurs. Hence, the same crystals have been observed during at least two weeks. This suggests that the crystals are in equilibrium with their environment despite frequent changes of the atmospheric conditions.

To remove hoar from the surface, the only effective processes are mechanical destruction and fast sublimation by the wind, or burying. Example of the later process is given in Sect. 3.3. The former process is the most common and is caused by particular wind conditions which are investigated in the remainder of this section.

We call "hoar disappearance event" (HDE) the change of surface state from hoar to smooth, and define the date of an HDE as the first day where the surface is classified as smooth. Figure 9 shows an example of a hoar disappearance event along with wind direction and speed. Between 8 and 9 February 2010, the wind direction changed from 215° (close to the southwest direction) to 105° (close to the east direction), and the wind speed increased by a factor two. Clouds were present on 8 February, explaining the gap in the time series of surface state. This particular event shows that both wind direction and speed changes may be involved in the disappearance of hoar.

To test the generality of this hypothesis, wind roses are plotted using all the data over the 18 months (Fig. 10a), using the data when hoar is present (Fig. 10b), and using only data coincident with HDE (Fig. 10c). The prevailing origin of the wind at Dome C is south-southwest. Altogether the directions from south to southwest correspond to 45 % of the days. The mean wind speed is 2.9 m s^{-1}. The wind rose when the hoar is present is similar to the wind rose using all the data over the 18 months, and the mean wind speed is only slightly lower 2.5 m s^{-1}.

In contrast, during HDE over the 18 months, the wind comes in general from the southeast and south-southeast (52 %). This represents a direction change of 70°, i.e. nearly a right angle. The wind speed 4.7 m s^{-1} is higher than normal. The three wind roses show that a relatively strong wind is required to remove the hoar, but it is not a sufficient condition. The wind direction is another crucial factor, at least over the period analysed here (see difference over the longer period in Sect. 3.2). The hoar disappearance requires wind from the southeast direction which is almost perpendicular to the prevailing wind and therefore perpendicular to the prevailing sastrugi direction (which is clearly visible in the field).

This observation suggests that the mechanical destruction (or very fast sublimation by the wind) of hoar crystals requires important kinetic energy which can only be supplied by intense turbulence. The turbulence near the surface is promoted not only by strong wind but also by high aerodynamic roughness length (Gallee et al., 2001; Van den Broeke et al., 2005). Because of the sastrugi (10 cm high at Dome C), this variable depends on wind direction and is probably higher at Dome C along the northwest–southeast axis than in the perpendicular, prevailing wind direction. It results that strong winds blowing parallel to the sastrugi prevailing direction may be less efficient for hoar removal than moderate winds blowing perpendicular to this direction. In the next section, this result based on only 19 HDE events, is extended over a longer period.

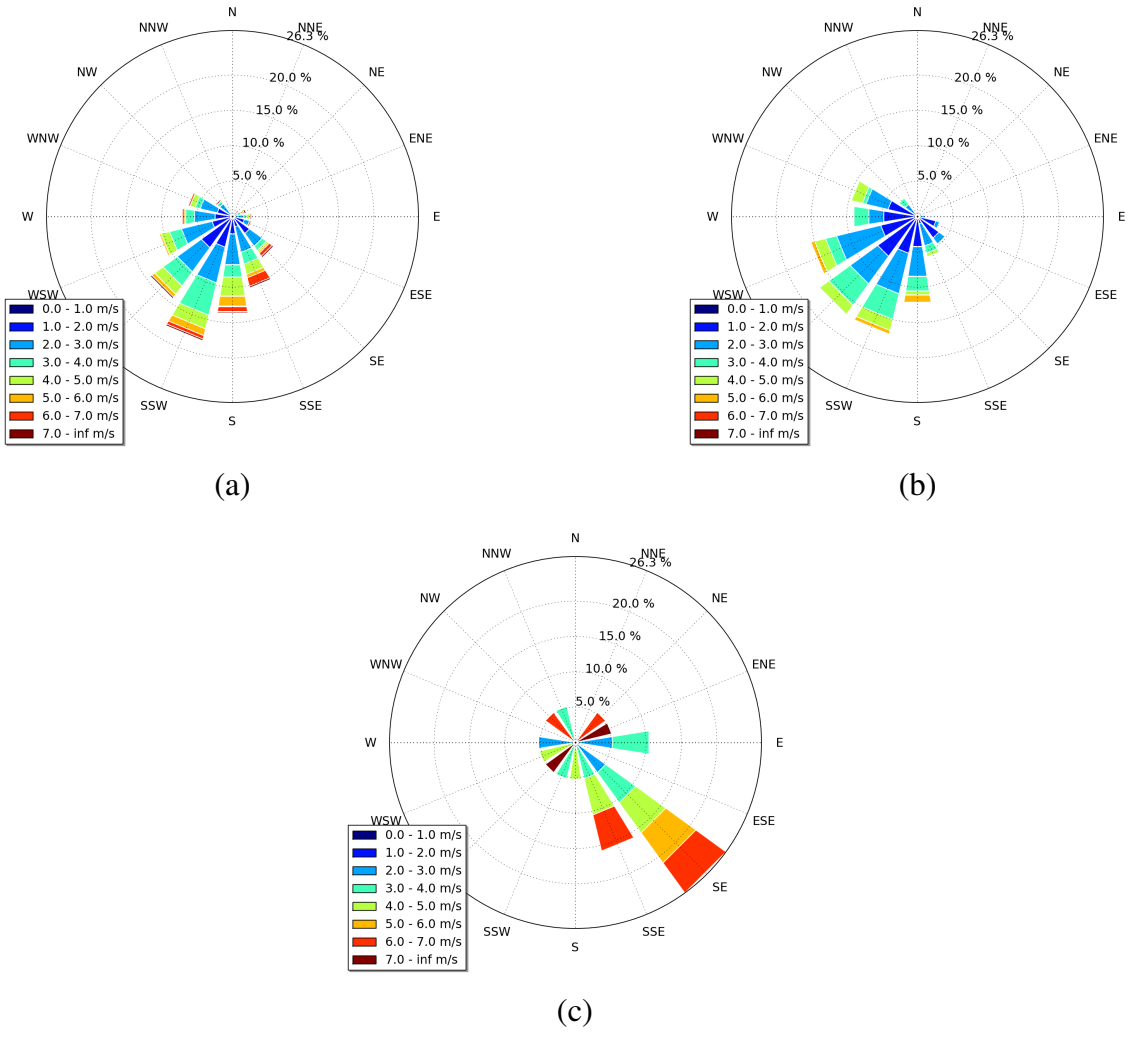

Fig. 10. Wind roses at Dome C **(a)** during the entire period of near-infrared pictures (from 23 November 2009 to 16 February 2010, and from 3 January 2011 to 11 April 2012), **(b)** when hoar is present, and **(c)** the set of days when hoar disappears. The cardinal direction is the origin of the wind.

3.2 Extension using passive microwave satellite observations

To extend the time series of surface state and the results concerning the development and disappearance of hoar, we use passive microwave data. We first present the time series of polarisation ratio derived from the AMSR-E observations, then show their correlation to the photography data and third analyse the time series over nearly 10 yr.

3.2.1 General characteristics

Figure 11 shows the time series of polarisation ratios (PR_{19} and PR_{37}) calculated from the AMSR-E observations. The difference of values between PR_{19} and PR_{37} is due to the layering of snow density within the snowpack and the higher penetration depth at 19 than at 37 GHz (Surdyk, 2002a,b).

The evolution of PR is a superimposition of quick and abrupt changes (1), a seasonal cycle (2) and a multi-annual increase trend (3). The evolution of PR mainly depends on snow density near the surface (see Sect. 2.2). The long-term trend (3) is significant (PR_{19} and PR_{37} increases are, respectively 0.0319 and 0.0325 in 10 yr), and could therefore be a progressive decrease of the near-surface density. However, we cannot either exclude a long-term evolution of snow density layering, surface roughness or temperature. This multi-annual trend is not explored in this study which focuses on hoar presence. The seasonal cycle (2) reveals a lower snow density near the surface in summer than in winter, and may be related to more developed hoar crystals at the surface in summer (see Sect. 3.1). Quick and rapid changes of polarisation ratios (3) are explored in the following two sections.

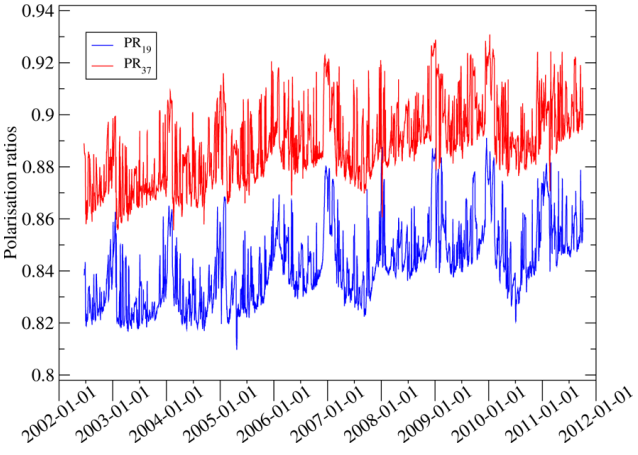

Fig. 11. Time series of polarisation ratios at 19 and 37 GHz at Dome C, from 19 June 2002 to 3 October 2011.

3.2.2 Correlation between passive microwave satellite and ground-based photography

Figures 7 and 8 show the evolution of PR_{19} and PR_{37} as well as the presence/absence of hoar. In general, the polarisation ratios are higher when hoar is detected by infrared photography. This was already noticed in Greenland by Shuman et al. (1993) and Shuman and Alley (1993), and is physically explained by the relationship between the high polarisation ratio, low density and presence of hoar. However, two short periods do not follow this general behaviour: (1) from 15 to 18 May 2011, the polarisation ratios increase while the surface remains smooth, and (2) from 29 to 31 May 2011, where the polarisation ratios are constant while hoar was developing (periods are marked (1) and (2) in Fig. 8). In case (1), visual inspection of the pictures provides a possible explanation: crystals were forming but they were small, i.e. too small to be detected by our algorithm. In case (2), sparse hoar crystals were present and were detected by the algorithm but they may have been insufficient to affect the snow density near the surface. The comparison over the entire series where pictures were available confirms the general correlation: the averages of polarisation ratios are higher when hoar is detected ($\overline{PR_{19}} = 0.866 \pm 0.012$ and $\overline{PR_{37}} = 0.911 \pm 0.010$) than when the surface is smooth ($\overline{PR_{19}} = 0.854 \pm 0.0069$ and $\overline{PR_{37}} = 0.898 \pm 0.0079$). However, a classification based on PR values is insufficient since the two classes (presence of hoar and smooth) largely overlap.

To investigate hoar disappearance, a better approach consists in detecting the change of polarisation ratio. For this, we compute the time derivatives of polarisation ratios with a one-day time lag. Figure 9 shows that highly negative values of the time derivations of PR_{19} and PR_{37} coincide with hoar disappearance. To detect automatically these negative values, we determined two thresholds (at 19 GHz and 37 GHz) by using all the hoar disappearance events detected by near-infrared photography. The resulting thresholds are 0.006 and 0.005 day^{-1} at 19 and 37 GHz, respectively.

Table 1. Contingency table of hoar disappearance events (detected by near-infrared photography) and polarisation ratio decreases (i.e. increase of snow density near the surface) during the common periods (from 23 November 2009 to 16 February 2010, and from 3 January 2011 to 3 October 2012).

	AMSR-E density increases	AMSR-E no density increases
PAuto HDE	10	5
PAuto no HDE	9	253

The snow density changes detected by satellite are compared with the hoar disappearance events detected by photography during the 18 months in common. Table 1 shows the contingency matrix: ten events are detected by both techniques. Five events of hoar crystal disappearance are missed by the satellite. In all cases, hoar crystals were sparse on the snow surface before the disappearance, which suggests the changes in density were too weak to be detected by satellite. These cases are similar to case (2) in Fig. 8 and cannot be considered to be failures of the satellite-based detection algorithm since the hoar was not well developed. In contrast, the nine events detected by the satellite and missed by PAuto (see Table 1), correspond to snow density changes without hoar disappearance events. For eight of them, the pictures of the previous days show very small crystals looking like fresh snow but no hoar crystals. Our hypothesis is that these events are not related to hoar, they result instead from the compaction of a recent snowfall by wind (Zwaaftink et al., 2012) which increased the apparent near-surface density. The last event is not understood.

Even though the events of polarisation ratio decrease are not strictly associated with hoar disappearance events, the correlation is significant and the analysis of the weather conditions responsible for these decreases is helpful.

3.2.3 Wind conditions associated with polarisation ratio decrease

Because snow metamorphism is slow on the East Antarctic Plateau, rapid increases of snow density near the surface can only be caused by the wind. To test this assumption, wind roses are plotted for the entire satellite period and for the set of dates where the polarisation ratios (at 19 and 37 GHz) decrease, ie. snow density near the surface increases (respectively Fig. 12a, b). As for the hoar disappearance events, an increase of wind speed and a change in wind direction is observed during density increase events. The mean wind speed is 4.9 m s^{-1} for the set of dates with density increases, instead of 3.2 m s^{-1} for the entire satellite period. More specifically, the occurrence of wind speeds greater than 4 m s^{-1} strongly increases, from 28 % for the entire satellite period

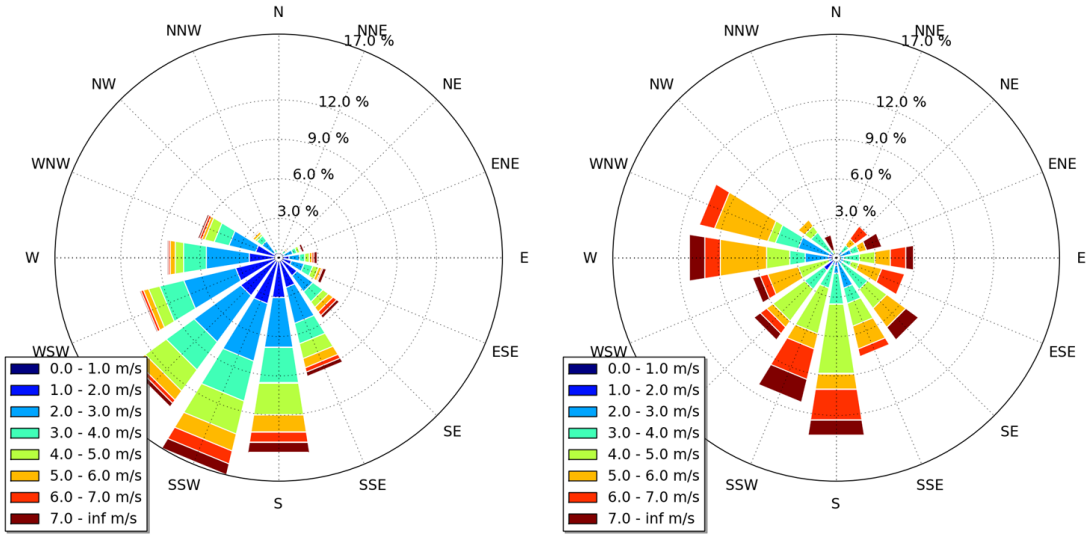

Fig. 12. Wind roses at Dome C **(a)** during the entire AMSR-E period from 19 June 2002 to 3 October 2011, and **(b)** during the events of snow density increases estimated with AMSR-E.

to more than 70 % for the set of dates when the snow density near the surface increases. The wind origins are clearly different during the density increase events from those under mean conditions. Winds from west to west-northwest appear to be favourable to the density increase events while the opposite direction is observed in the case of hoar disappearance during the photography period. In both cases, the direction is almost perpendicular to the prevailing wind direction which is compatible with a significant role of the aerodynamic roughness length. There was no occurrence of wind coming from the prevailing direction (south-southwest to south) in the case of hoar disappearance while it is frequent in the case of density increases. This is not surprising since the formation of sastrugi in the prevailing direction requires compaction and scouring by wind in this direction. The absence of the south-southwest prevailing direction in Fig. 10 is most probably a consequence of the statistically small size of the HDE set.

Despite the differences of nature between the satellite time series and hoar disappearance events, the results in both cases show the dominant role of the wind speed – with a threshold level around $4\,\mathrm{m\,s^{-1}}$ – and more originally, an important role of the winds blowing perpendicularly to the prevailing direction.

3.3 Interaction between hoar crystals and snowfall

For 4–5 out of the 19 events of hoar disappearance, a detailed analysis of the infrared pictures provides evidence of burying of the crystals instead of mechanical destruction and transport. The event on 8 and 9 February 2010 (marked B in Figs. 7, 9, 13 and 14) is investigated in detail.

Figures 13 and 14 show the time series of several variables during 9 days around the event. According to the detection algorithm, hoar was present until the day 7, the day 8 was cloudy, which explains the gaps in the infrared photography data, and on day 9 the hoar had disappeared. Snowfalls were detected locally by a disdrometer installed around 2 m above the snow surface (such as BIRAL VPF730 in Bellot et al., 2011), about 50 m from PAuto, and were forecasted by the ERA-Interim reanalysis (Simmons et al., 2006). Figure 15a and b show the surface seen by Pauto before and after the event. Before, the hoar was well developed and covered the whole surface. After the event, our algorithm considered that the hoar had disappeared but a few individual snow crystals remained visible after and emerged above the freshly deposited snow. This new snow has small particles as is confirmed indirectly by the broadband albedo time series (Fig. 14). The albedo – calculated by the ratio of upward on downward short wave radiations measured by the World Radiation Monitoring Center – Baseline Surface Radiation Network – increases sharply during the event and decreases afterwards but remains higher than before the event. The peak may be due to the cloudy condition, and the fact that snow albedo is generally higher under diffuse illumination and if falling ice crystals are present in the air (Warren, 1982). The higher value of the albedo after the event suggests that the snowfalls deposited grains with a smaller optical radius.

The polarisation ratio at both frequencies decreases during the period (Fig. 9), revealing an increase of the near-surface density. According to the picture, a possible explanation is that snowfalls (or drifting snow) brought small particles that were easily captured by the hoar or fell in the gaps available between the crystals. Hence, the density increased because matter was added without a significant change of the surface

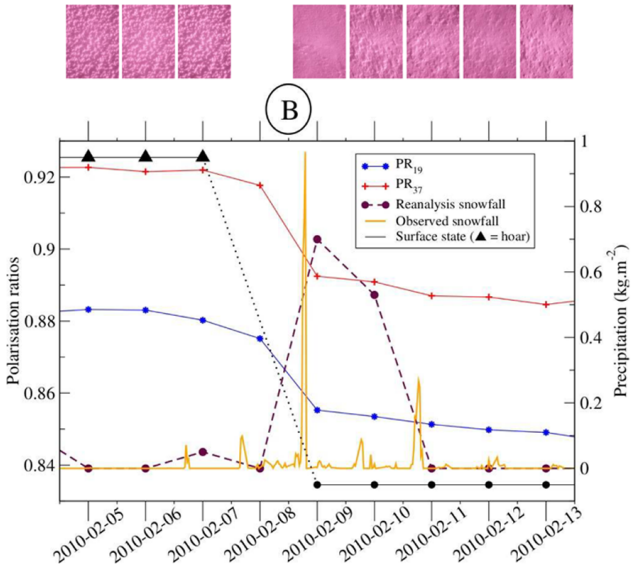

Fig. 13. Observed and forecasted snowfall on 9 February 2010 at Dome C, during the disappearance of hoar crystals (unscaled black symbols and small pictures above the graph) present on the snow surface (event B in Fig. 7). Between the 8 and 9, a decrease of polarisation ratios at 19 and 37 GHz is also observed.

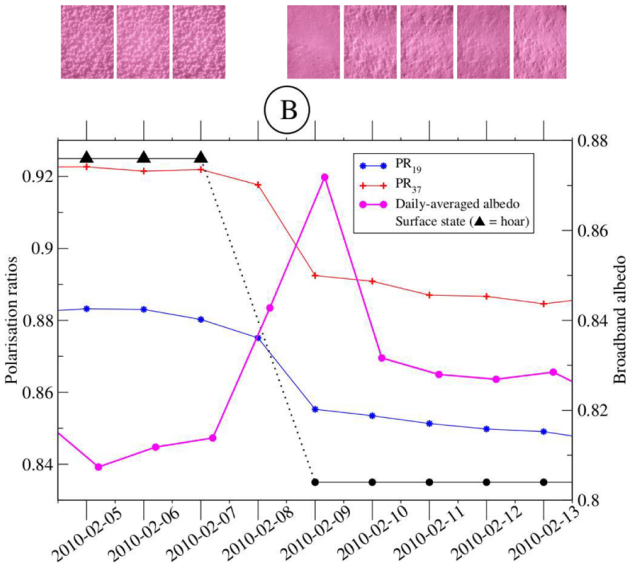

Fig. 14. Observed albedo on 8 and 9 February 2010 at Dome C, during the disappearance of hoar crystals (unscaled black symbols and small pictures above the graph) present on the snow surface (event B in Fig. 7). Between the 8 and 9, a decrease of polarisation ratios at 19 and 37 GHz is also observed.

elevation (only a slight net accumulation is observed on the two vertical stakes). Compared with the case of a smooth surface, this process of snow settling in the presence of hoar is very efficient because once fallen within the structure, the particles can be less easily captured by the air flow. In addition, the particles may contribute to the densification and consolidation of the whole structure. Even if wind speed increases, the particles and the hoar will more likely resist.

Similar events were observed throughout the year: on 8 January 2011, 25 April 2011 and 22 July 2011, with clouds clearly present during most events. Another event, on 17 August 2011 was intermediate as partial destruction of the hoar by wind seems to occur. This process, i.e. snowfall (or drifting snow) captured by the hoar, could also apply with clear-sky precipitation (diamond dust), the very small precipitating particles formed by radiative cooling air often observed on the East Antarctic Plateau (Schwerdtfeger, 1969, 1984; Bromwich, 1988; Walden et al., 2003). However, we have no evidence of this phenomenon with PAuto.

The pictures before and after the event of the 8 January 2011 (Fig. 16) show more clearly the preferential capture of the fresh snow by the hoar present at the surface. Finally, with 1–2 cm-high hoar crystals and annual accumulation around 8 cm (i.e. 30 kg m^{-2} water equivalent in Van de Berg et al., 2006) at Dome C, this process might well play a significant role in the spatial distribution of snow accumulation. Where and when hoar is developed, snow settling is more likely and thus accumulation could be greater.

4 Conclusions

An 18 month-long time series of daily presence of hoar crystals at Dome C was derived from in situ near-infrared photographs using an automatic algorithm based on image texture analysis. Hoar is present on the surface almost half of the time (45 %) at Dome C all year round. The nature of these crystals is either "surface hoar" formed by condensation of the air water vapour onto the surface or frost flower-like crystals formed by upwelling vapour emanating from the snow a few centimetres under the surface. New observations and modelling is required to specify the nature and the conditions of hoar formation. The development of the crystals is progressive (typically 4–5 days) while the disappearance is always rapid and associated with particular weather conditions. Wind is an important factor, a speed of at least 4 m s^{-1} is required to remove the hoar from the surface. More surprisingly, our observations show that most events of hoar disappearance occur when the wind blows perpendicularly to the prevailing wind direction. We interpret this by the larger turbulent kinetic energy near the surface when wind blows perpendicularly to the sastrugi, which are usually aligned along the prevailing wind direction. Measurements of the aerodynamic roughness length via high-resolution vertical profiling of the wind speed near the surface could confirm whether the dependence of hoar disappearance on wind direction is caused by the turbulence.

Passive microwave satellite observations are known to be sensitive to the presence of hoar when the brightness temperature at horizontal and vertical polarisations are combined.

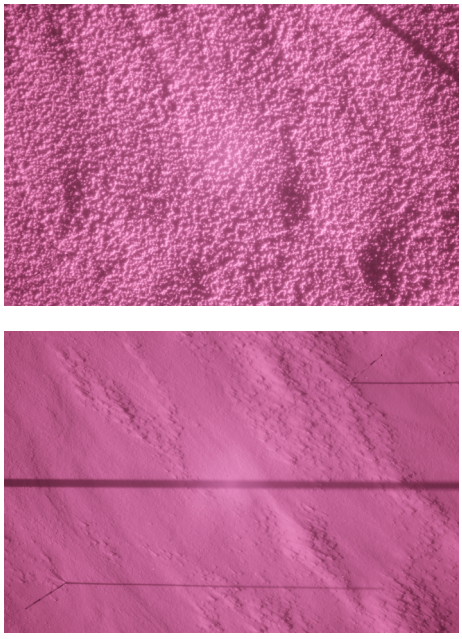

Fig. 15. Near-infrared pictures at Dome C before and after hoar disappearance caused by burying or capture of fresh snow. Event B: **(a)** 7, and **(b)** 9 February 2010.

The comparison of the polarisation ratio time series at Dome C to the near-infrared photography confirms this sensitivity and also draws a more complex picture: the polarisation ratio depends fundamentally on the snow density near the surface which increases not only when hoar disappears (10 events among 19) but also when fresh snow is compacted by wind events (8 events among 19). Over the 10 year-long satellite time series, we found that both wind speed and direction are important factors leading to a density increase whether it results from hoar disappearance or fresh snow compaction.

In addition, evidence of snowfalls during hoar crystal disappearance events was also identified in some near-infrared pictures. Fresh snow particles could easily be captured by the hoar, which would promote snow settling by densification and sheltering from the air flow. Since the snow depth accumulated every year at Dome C is only 4–8 times the typical hoar height, this process of capture could be significant and enhance accumulation where and when hoar is present. Altogether these results demonstrate the complex interactions between hoar, sastrugi, snow settling, accumulation, wind speed and wind direction.

Acknowledgements. This work was supported by the Programme National de Télédétection Spatiale and the Agence Nationale de la Recherche (MONISNOW ANR-11-JS56-005-01). We thank the French polar institute (Institut Paul-Émile Victor) for logistical support through CALVA and TASTE-IDEA programs. We thank the following institutes for providing data: the European Centre for Medium-range Weather Forecasts (ERA Interim), Antarctic Meteorological Research Center (weather observation), the National Snow and Ice Data Center (satellite data) and the Baseline Surface Radiation Network (radiation observations). We also thank C. Genthon and D. Six, LGGE, for the disdrometer data.

Edited by: A. Klein

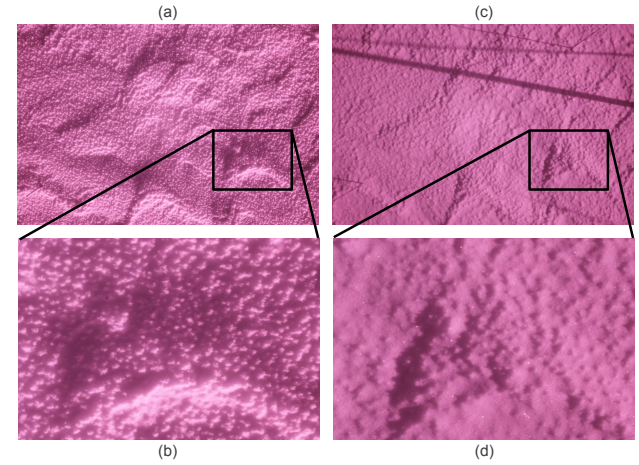

Fig. 16. Near-infrared pictures at Dome C before and after hoar disappearance caused by burying or capture of fresh snow. **(a)** and **(b)** 7, **(c)** and **(d)** 9 January 2011.

The publication of this article is financed by CNRS-INSU.

References

Arthern, R. J., Winnebrenner, D. P., and Vaughan, D. G.: Antarctic snow accumulation mapped using polarization of 4.3 cm wavelength microwave emission, J. Geophys. Res., 111, doi:10.1029/2004JD005667, 2006.

Bellot, H., Trouvilliez, A., Naaim-Bouvet, F., Genthon, C., and Gallée, H.: Present weather-sensor tests for measuring drifting snow, Ann. Glaciol., 52, 176–184, doi:10.3189/172756411797252356, 2011.

Born, M. and Wolf, E.: Principles of Optics Electromagnetic, Theory of Propagation, Interference and Diffraction of Light, Cambridge University Press, Cambridge, 1999.

Bromwich, D. H.: Snowfall in High Southern Latitudes, Rev. Geophys., 26, 149–168, 1988.

Brucker, L., Picard, G., Arnaud, L., Barnola, J.-M., Schneebeli, M., Brunjail, H., Lefebvre, E., and Fily, M.: Modeling time series of microwave brightness temperature at Dome C, Antarctica, using vertically resolved snow temperature and microstructure measurements, J. Glaciol., 57, 171–182, doi:10.3189/002214311795306736, 2011.

Brun, E., Six, D., Picard, G., Vionnet, V., Arnaud, L., Bazile, E., Boone, A., Bouchard, A., Genthon, C., Guidard, V., Le Moigne,

P., Rabier, F., and Seity, Y.: Snow/atmosphere coupled simulation at Dome C, Antarctica, J. Glaciol., 57, 721–736, doi:10.3189/002214311797409794, 2011.

Colbeck, S.: Theory of Metamorphism of Dry Snow, J. Geophys. Res., 88, 5475–5482, doi:10.1029/JC088iC09p05475, 1983.

Di Siquiera, F. R., Schwartz, W. R., and Pedrini, H.: Multi-scale Gray Level Co–Occurence Matrices for Texture Description, Neurocomputing, 2013.

Domine, F. and Shepson, P. B.: Air-Snow Interactions and Atmospheric Chemistry, Science, 297, 1506–1510, doi:10.1126/science.1074610, 2002.

Domine, F., Taillandier, A. S., Simpson, W. R., and Severin, K.: Specific surface area, density and microstructure of frost flowers, Geophys. Res. Lett., 32, 13502, doi:10.1029/2005GL023245, 2005.

Domine, F., Salvatori, R., Legagneux, L., Salzano, R., Fily, M., and Casacchia, R.: Correlation between the specific surface area and the short wave infrared (SWIR) reflectance of snow, Cold Reg. Sci. Technol., 46, 60–68, doi:10.1016/j.coldregions.2006.06.002, 2006.

Domine, F., Gallet, J.-C., Bock, J., and Morin, S.: Structure, specific surface area and thermal conductivity of the snowpack around Barrow, Alaska, J. Geophys. Res., 117, D00R14, doi:10.1029/2011JD016647, 2012.

Eisen, O., Frezzotti, M., Genthon, C., Isaksson, E., Magand, O., Van den Broeke, M. R., Dixon, D. A., Ekaykin, A., Holmlund, P., Kameda, T., Karlöf, L., Kaspari, S., Lipenkov, V., Oerter, H., Takahashi, S., and Vaughan, D. G.: Ground-based measurements of spatial and temporal variability of snow accumulation in East Antarctica, Rev. Geophys., 46, 1–39, doi:10.1029/2006RG000218, 2008.

Favier, V., Agosta, C., Genthon, C., Arnaud, L., Trouvillez, A., and Gallée, H.: Modeling the mass and surface heat budgets in a coastal blue ice area of Adelie Land, Antarctica, J. Geophys. Res., 116, F03017, doi:10.1029/2010JF001939, 2011.

Fierz, C., Armstrong, R., Durand, Y., Etchevers, P., Greene, E., McClung, D., Nishimura, K., Satyawali, P., and Sokratov, S.: The International Classification for Seasonal Snow on the Ground, Tech. Rep. 83, UNESCO, 2009.

Flanner, M. G. and Zender, C. S.: Linking snowpack microphysics and albedo evolution, J. Geophys. Res., 111, D12208, doi:10.1029/2005JD006834, 2006.

Gallee, H., Guyomarc'h, G., and Brun, E.: Impact of snow drift in the Antarctic ice sheet surface mass balance: possible sensitivity to snow surfaces properties, Bound.-Lay. Meteoro., 99, 1–19, doi:10.1023/A:1018776422809, 2001.

Gallet, J.-C., Domine, F., Arnaud, L., Picard, G., and Savarino, J.: Vertical profile of the specific surface area and density of the snow at Dome C and on a transect to Dumont D'Urville, Antarctica – albedo calculations and comparison to remote sensing products, The Cryosphere, 5, 631–649, doi:10.5194/tc-5-631-2011, 2011.

Gardner, A. S. and Sharp, M. J.: A review of snow and ice albedo and the development of a new physically based broadband albedo parameterization, J. Geophys. Res., 115, F01009, doi:10.1029/2009JF001444, 2010.

Gow, A. J.: On the accumulation and seasonal stratification of snow at the South Pole, J. Glaciol., 5, 467–477, 1965.

Hall-Beyer, M.: GLCM Texture: A Tutorial, 2007.

Haralick, R. M., Shanmugam, K., and Dinstein, I.: Textural Features for Image Classification, Transactions on Systems, Man and Cybernetics, 3, 610–620, doi:10.1109/TSMC.1973.4309314, 1973.

He, D.-C., Wang, L., and Guibert, J.: Texture discrimination based on an optimal utilization of texture features, Pattern Recogn., 21, 141–146, doi:10.1016/0031-3203(88)90020-9, 1988.

Lacroix, P., Legrésy, B., Rémy, F., Blarel, F., Picard, G., and Brucker, L.: Rapid change of snow surface properties at Vostok, East Antarctica, revealed by altimetry and radiometry, Remote Sens. Environ., 113, 2633–2641, doi:10.1016/j.rse.2009.07.019, 2009.

Liang, D., Xu, X., Tsang, L., Andreadis, K. M., and Josberger, E. G.: The Effects of Layers in Dry Snow on Its Passive Microwave Emissions Using Dense Media Radiative Transfer Theory Based on the Quasicrystalline Approximation (QCA/DMRT), IEEE T. Geosci. Remote, 46, 3663–3671, doi:10.1109/TGRS.2008.922143, 2008.

Liang, D., Xu, P., Tsang, L., Gui, Z., and Chen, K.: Electromagnetic scattering by rough surfaces with larges heights and slopes with applications to microwave remote sensing of rough surface over layered media, Prog. Electromagn. Res., 95, 199–218, doi:10.2528/PIER09071413, 2009.

Linkletter, G. O. and Warburton, J. A.: Short notes. A note of the contribution of rime and surface hoar to the accumulation on the Ross ice shelf, Antarctica, J. Glaciol., 17, 351–353, 1976.

Long, D. G. and Drinkwater, M. R.: Azimuth Variation in Microwave Scatterometer and Radiometer Data Over Antarctica, IEEE T. Geosci. Remote, 38, 1857–1870, doi:10.1109/36.851769, 2000.

Macelloni, G., Brogioni, M., Pampaloni, P., and Cagnati, A.: Multifrequency Microwave Emission From the Dome-C Area on the East Antarctic Plateau: Temporal and Spatial Variability, IEEE T. Geosci. Remote, 45, 2029–2039, doi:10.1109/TGRS.2007.890805, 2007.

Mätzler, C.: On the Determination of Surface Emissivity From Satellite Observations, IEEE Geo. Rem. Sens. Lett., 2, 160–163, doi:10.1109/LGRS.2004.842448, 2005.

Orheim, O.: Surface snow metamorphosis on the Antarctic Plateau, Norks Polarinstitutt, Arbok 1966, 84–91, 1968.

Picard, G., Brucker, L., Fily, M., Gallée, H., and Krinner, G.: Modeling time series of microwave brightness temperature in Antarctica, J. Glaciol., 55, 537–551, doi:10.3189/002214309788816678, 2009.

Picard, G., Domine, F., Krinner, G., Arnaud, L., and Lefebvre, E.: Inhibition of the positive snow-albedo feedback by precipitation in interior Antarctica, Nat. Clim. Change, 2, 7, doi:10.1038/nclimate1590, 2012.

Plataniotis, K. N. and Venetsanopoulos: Color Image Processing and Applications, 2000.

Saunders, W., Lawrence, J. S., Storey, J. W. V., and Ashley, M. C. B.: Where Is the Best Site on Earth? Domes A, B, C and F, and Ridges and B, Publications of the Astronomical Society of the Pacific, 121, 976–992, 2009.

Schwerdtfeger, W.: Ice Crystal Precipitation on the Antarctic Plateau, Antarctic Journal of the U.S., 4, 221–222, 1969.

Schwerdtfeger, W.: Weather and the climate of the Antarctic, Elsevier, Amsterdam, 1984.

Serra, J.: Image Analysis and Mathematical Morphology, Volume 1, vol. 1, Academic Press, Orlando, 1984.

Serra, J.: Image Analysis and Mathematical Morphology, Volume 2: Theoritical Advances, vol. 152, Blackwell Science Ltd, doi:10.1111/j.1365-2818.1988.tb01425.x, 1988.

Sherjal, I. and Fily, M.: Temporal variations of microwave brightness temperatures over Antarctica, Ann. Glaciol., 20, 19–25, 1994.

Shuman, C. A. and Alley, R. B.: Spatial and temporal characterization of hoar formation in central Greenland using SSM/I brightness temperatures, Geophys. Res. Lett., 20, 2643–2646, doi:10.1029/93GL02810, 1993.

Shuman, C. A., Alley, R. B., and Anandakrishnan, S.: Characterization of a hoar-development episode using SSM/I brightness temperatures in the vicinity of GISP2 site, Greenland, Ann. Glaciol., 17, 183–188, 1993.

Simmons, A., Uppala, S., Dee, D., and Kobayashi, S.: ERA-Interim: New ECMWF reanalysis products from 1989 onwards, ECMWF Newsletter, 110, 26–35, 2006.

Slaughter, A., Adams, E., Straron, P., Shertzer, R., Walters, D., D., M., Catherine, D., Henninger, I., Leonard, T., Cooperstein, M., and H., M.: Field investigation of near-surface metamorphism of snow, J. Glaciol., 57, 441–452, doi:10.3189/002214311796905695, 2011.

Style, R. W. and Worster, M. G.: Frost flower formation on sea ice and lake ice, Geophys. Res. Lett., 36, L11501, doi:10.1029/2009GL037304, 2009.

Surdyk, S.: Using microwave brightness temperature to detect short-term surface air temperature changes in Antarctica: An analytical approach, Remote Sens. Environ., 80, 256–271, doi:10.1016/S0034-4257(01)00308-X, 2002a.

Surdyk, S.: Low microwave brightness temperatures in central Antarctica: observed features and implications, Ann. Glaciol., 34, 134–140, doi:10.3189/172756402781817464, 2002b.

Surdyk, S. and Fily, M.: Comparison of the passive microwave spectral signature of the Antarctic ice sheet with ground traverse data, Ann. Glaciol., 17, 161–166, 1993.

Taillandier, A.-S., Domine, F., Simpson, W. R., Sturm, M., and Douglas, T. A.: The rate of decrease of the specific surface area of dry snow: Isothermal versus temperature gradient conditions, J. Geophys. Res., 112, doi:10.1029/2006JF000514, 2007.

Town, M. S., Waddington, E. D., Walden, V. P., and Warren, S. G.: Temperatures, heating rates, and vapour pressures in the near-surface snow at South Pole, J. Glaciol., 54, 487–498, 2008.

Tsang, L., Chen, C.-T., Chang, A. T., Guo, J., and Ding, K.-H.: Dense media radiative transfer theory based on quasicrystalline approximation with application to passive microwave remote sensing of snow, Radio Sci., 35, 741–749, doi:10.1029/1999RS002270, 2000.

Van de Berg, W. J., van den Broeke, M. R., Reijmer, C. H., and van Meijgaard, E.: Reassessment of the Antarctic surface mass balance using calibrated output of a regional atmospheric climate model, J. Geophys. Res., 111, D11104, doi:10.1029/2005JD006495, 2006.

Van den Broeke, M., Van As, D., Reijmer, C., and Van de Wal, R.: Sensible heat exchange at the Antarctic snow surface: a study with automatic weather stations, Int. J. Climatol., 25, 1081–1101, doi:10.1002/joc.1152, 2005.

Walden, V. P., Warren, S. G., and Tuttle, E.: Atmospheric Ice Crystals over the Antarctic Plateau in Winter, J. Appl. Meteorol., 42, 1391–1405, 2003.

Warren, S. G.: Optical Properties of Snow, Rev. Geophys. Space Phys., 20, 67–89, doi:10.1029/RG020i001p00067, 1982.

Weidner, G. A.: Technical Manual for Automatic Weather Stations, Tech. rep., Department of Meteorology, Unviersity of Wisconsin-Madison, Wisconsin-Madison, 1985.

Weller, G.: The heat and mass balance of snow dunes on the Central Antarctic Plateau, J. Glaciol., 8, 277–284, 1969.

Zwaaftink, C. D., Cagnati, A., Crepaz, A., Fierz, C., Lehning, M., Macelloni, G., and Valt, M.: Event-driven deposition: a new paradigm for snow-cover moelling in Antarctica based on surface measurements, 3575–3612, 2012.

Zwally, H. J.: Microwave emissivity and accumulation rate of polar firn, J. Glaciol., 18, 195–214, 1977.